L-norepinephrine induces ROS formation but alters microbial community composition by altering cellular metabolism

Amrita Bains[1,†], Sanjeev Dahal[2,†], Bharat Manna[1†], Mark Lyte[3], Edward P. Kolodziej[4,5], Frank W.R. Chaplen[6], Laurence Yang[2], Naresh Singhal[1,*]

[1] Department of Civil and Environmental Engineering, University of Auckland, Auckland, New Zealand

[2] Faculty of Engineering and Applied Science, Queen's University, Ontario, Canada

[3] Department of Veterinary Microbiology & Preventive Medicine, Iowa State University, Iowa, USA

[4] Center for Urban Waters, Tacoma, Washington, United States

[5] Department of Civil & Environmental Engineering, University of Washington, Washington, USA

[6] Biological and Ecological Engineering, Oregon State University, Corvallis, OR 97331, USA

[†]Authors contributed equally to the paper

[*]Corresponding author: Email: n.singhal@auckland.ac.nz

ABSTRACT

Catecholamines, such as L-norepinephrine (L-NE), are naturally present in the human gut and are discharged into the sewage. The bioactivity of L-NE can significantly alter the speciation and function of the microbial community by stimulating bacterial growth and producing H_2O_2. The accompanying changes in intracellular metabolism could significantly impact biological wastewater treatment processes, but they have remained unexplored. We investigate the alterations by L-NE and two other Catecholamines (Dopamine, and L-Dopa) to microbial consortia sourced from a dairy farm settling pond (FS) and the activated sludge of a municipal wastewater treatment plant (MS). We contrast the effect of the catecholamines on these mixed microbial communities with dextrose, a readily degradable substrate, and elevated levels of intracellular H_2O_2 through high dissolved oxygen (HDO) perturbations and exogenous applications of paraquat (PQ) and hydrogen peroxide (H_2O_2). The microbial community composition in different catecholamines was similar to the Dextrose treatment. However, there were significant changes in the PQ and H_2O_2 supplemented systems. In addition, the functional potential of the microbial communities with catecholamines and Dextrose were similar and provided insight into metabolic shifts from the control systems. While exogenous H_2O_2 increased the abundance of *Rhodocyclaceae*, *Flavobacteriaceae* and *Chitinophagaceae* and others, L-NE paralleled dextrose by increasing *Pseudomonadaceae*, *Moraxellaceae*, and *Sphingobacteriaceae* in the microbial consortia. A number of protein functions related to oxidoreductase, peroxidase, and catalase activities, ATP and FAD/$FADH_2$ binding, nitrate reductase, and glutamate-ammonia ligase activity were differentially expressed by L-NE over dextrose, but many of the ROS-scavenging functions were overexpressed in the exogenous H_2O_2 treatment over L-NE. A proteome-constrained flux balance analysis showed that in comparison to dextrose, L-NE increased the fluxes of gluconeogenesis, glycolysis, oxidative stress metabolism, and glutamate metabolism. L-NE increases stress tolerance and microbial growth by upregulating the activities of oxidative stress mitigating enzymes (catalase and thioredoxin) and nitrogen assimilation activities (glutamine formation).

Keywords: catecholamine, functional potential, targeted proteomics, pseudomonas putida kt2440, M-model simulations, archetypal analysis

Introduction

Catecholamines are produced by the enzymatic oxidation of the amino acid tyrosine in the mammalian brain, nerve tissues, and adrenal glands (Saller et al. 2012). These chemicals regulate many vital physiological and metabolic responses in the gut and contribute to human gut-brain communication (Lyte 2013). Previous studies on catecholamines have primarily examined microbiota interactions in the human gut (Eisenhofer et al. 1997; Freestone et al. 2008; Zhou, Hank Simms, and Wang 2004). Some studies have investigated pathogen colonization as norepinephrine and other catecholamines regulate several microbial functions relating to pathogenicity (Chen et al. 2003; Cogan et al. 2007; Nakano et al. 2007; Truccollo, Whyte, and Bolton 2020). L-norepinephrine (L-NE), a typical catecholamine, is a stress hormone that regulates crucial phenotypes for pathogen infections such as motility, growth, adhesion, biofilm formation, and virulence (Bansal et al. 2007; Gao et al. 2019; Sandrini et al. 2014; Sarkodie et al. 2019). L-NE addition causes rapid growth of Gram-negative bacteria (Kinney et al. 2000); Gram-positive bacteria also respond to L-NE, but most do not exhibit rapid growth (Freestone et al. 1999). However, some studies have reported adverse effects on microbial growth (Belay et al. 2003; Burton et al. 2002). The L-NE-associated stimulation of bacterial growth is not linear dose-dependent, occurring only when L-NE is above specific threshold concentrations (Gao et al. 2019). In addition to promoting growth, L-NE influences diverse cellular functions by upregulating gene expression for enzyme metabolism, DNA repair, metabolism, ribosomal protein biosynthesis, motility, and virulence (Gao et al. 2019; Xu et al. 2015). L-NE metabolism involves reactive oxygen species (ROS) such as superoxide ion radicals ($O_2^{\cdot-}$) and hydrogen peroxide (H_2O_2) (Maggiorani et al. 2017; Neri et al. 2007; Saller et al. 2012). These ROS can influence various cell fate decisions and signal transduction pathways, for example, through reversible oxidation and reduction of amino acids (Holmström and Finkel 2014). At the low physiological levels in the nanomolar range, these ROS are key signalling agents involved in metabolic regulation, activating numerous growth-supporting pathways (Bonavita and Laukkanen 2021; Sies 2017; Thannickal and Fanburg 2000). Applying sublethal levels of H_2O_2 to *Pseudomonas putida* reconfigures intracellular metabolism by redirecting periplasmic glucose processing to cytoplasmic oxidation and significantly increasing NADPH-forming fluxes to energize the glutathione system and decrease H_2O_2 (Nikel et al., 2021). However, elevated levels of ROS can oxidize proteins and damage biomolecules, causing growth arrest and cell death (Imlay 2013; Sies and Jones 2020; Yang et al. 2019). Interestingly, despite the production of ROS by cellular metabolism, L-NE induces

rapid growth of the microbial population. This interplay of the overall effect of ROS production and rapid microbial growth has not been previously examined and demands an in-depth investigation. In particular, if these conditions lead to the survival and proliferation of pathogens or alter the carbon and nitrogen metabolism, it could have significant consequences on the performance of biological processes in wastewater treatment. Deciphering the microbial responses to L-NE is necessary to gain insight into unacknowledged threats from uncharacterized bioactive substances naturally present in wastewater.

In this study, we explore the effects of catecholamines on the growth, speciation, and metabolism of the microbial communities. We assess the impact of three representative catecholamines (L-NE, Dopamine, and L-Dopa) on mixed microbial cultures from a dairy farm settling pond and the aerobic reactor of a municipal wastewater treatment plant in Auckland, New Zealand. Furthermore, we compare the shift in the microbial population under different catecholamine treatments with exogenous ROS application as well as under nutrient-rich conditions where dextrose was provided as an easily degradable substrate. Using these controls we interpret the impact of catecholamines on the compositional shift in the microbial communities via ROS formation and alteration in their metabolic functions. We adopt a top-down approach by implementing 16s rRNA-based taxonomic profiling of the metagenomes from different treatments to decipher the change in the microbial population, followed by inferring the functional potential of the microbial communities, and metaproteome-based confirmatory functional analysis. Finally, we investigate the specific effects of L-NE by performing the proteome-constrained flux balance analysis (FBA) to link the shifts in metabolic pathways to the observed microbial growth.

Material and Methods

Batch experiments

Sludge samples were collected from the settling pond at a dairy farm (FS) and activated sludge from a municipal wastewater treatment plant (MS) in Auckland, New Zealand. The microbial cultures were acclimated by adding 10 mL of sludge to 20 mL of synthetic wastewater containing 400 mg/L-COD of acetate, 60 mg-N/L of ammonium (was it added as ammonium chloride) supplemented with 25 mM of HEPES buffer (DI water), and incubated overnight at 37˚C on a rotating shaker. The acclimated cultures were centrifuged at 4,000 rpm for 10 min and washed twice with phosphate-buffered saline (PBS). We used a standard curve of A_{595} versus colony forming units (CFU) to seed 1L bioreactors to 100 CFU mL^{-1} with the washed

dairy farm and the wastewater treatment plant cultures as a final microbial concentration in the bioreactors. The final concentrations of bacteria inoculated into bioreactors were determined on tryptic soy agar (TSA) plates using standard pour-plate technique. Batch experiments were conducted using 1×10^{-5} M, 5×10^{-5} M and 1×10^{-4} M L-NE in bioreactors to simulate physiologically relevant L-NE levels observed *in vivo* (Lyte, Frank, and Green 1996). Tests with other catecholamines, L-DOPA and Dopamine, were also performed using procedure similar to L-NE at only one optimised concentration of 5×10^{-5} M. Reactors with similar dextrose levels served as controls for easily degradable carbon course, although this approach added 10X carbon in the dextrose controls compared to the corresponding L-NE reactors. Two bioreactors seeded with 50 μM paraquat (PQ) and 50 μM H_2O_2 added to municipal sludge cultures served as ROS control. All bioreactors were continuously mixed at 100 rpm on magnetic stirrers and operated at room temperature 22-25˚C for 24 h. The experimental conditions for the cultures tested are summarised in Table 1. The microbial growth in bioreactors was measured using the standard pour plate technique on tryptic soy agar (TSA) plates. The samples were collected at 0, 8 and 24 h. The 24 h samples were analysed in duplicate for bacterial growth, total abundance of ROS genes *oxyR* and *SoxRS*, proteins and microbial composition (Table S1). Additional methodological details (specify which methodologies) are provided in the Supplementary Information S1.1.

Table 1. Description of the experimental conditions tested in this study.

Experimental Condition	Description
High Dissolved Oxygen (HDO)	Base condition with the dairy farm and activated sludge cultures maintained in synthetic wastewater under constant aeration to maintain ~8 mg/L of dissolved oxygen.
Dextrose	The HDO cultures supplemented with $1x10^{-5}$ M, $5x10^{-5}$ M or $1x10^{-4}$ M dextrose to serve as metabolic carbon source control.
L-NE	The HDO cultures supplemented with 1×10^{-5}, 5×10^{-5} or 1×10^{-4} M L-NE.
Dopamine	The HDO cultures supplemented with 5×10^{-5} M Dopamine.
L-Dopa	The HDO cultures supplemented with 5×10^{-5} M L-Dopa.
PQ	The activated sludge culture maintained in synthetic wastewater media containing 50 μM paraquat to serve as ROS control.
H_2O_2	The activated sludge culture maintained in synthetic wastewater media containing 50 μM hydrogen peroxide as ROS control.

Microbial DNA isolation and Taxonomic Profiling

The composition of the bacterial community was characterised by amplifying and sequencing bacterial 16S ribosomal RNA (rRNA) gene fragments with the universal 16S PCR forward primer (5'-**TCGTCGGCAGCGTCAGATGTGTATAAGAGACAG**CCTACGGGNGGCWGCAG-3') and the 16S PCR reverse primer (5'-**GTCTCGTGGGCTCGGAGATGTGTATAAGAGACAG**GACTACHVGGGTATCTAA TCC-3') following a standard protocol (Quast et al. 2013); nucleotide bases in bold are Illumina overhang adapter sequences for high-throughput sequencing. Amplified PCR products were purified using an AMPure XP beads kit (Beckman Coulter Inc.) and DNA concentrations were recorded using a Qubit® dsDNA HS Assay Kit (Life Technologies) according to the manufacturer's instructions and then sequenced on an Illumina MiSeq machine (New Zealand Genomics Ltd., Auckland, New Zealand) using 2-by-300 bp chemistry. Before DNA sequencing, the sequencing provider attached a unique combination of Nextera XT dual indices (Illumina Inc., USA) to the DNA of each sample to allow multiplex sequencing. The resulting paired-end read DNA sequence data were merged and quality filtered using the USEARCH sequence analysis tool (Edgar 2013). Data was de-replicated so that only one copy of each sequence was retained. Sequence data were then checked for chimeric sequences and clustered into groups of operational taxonomic units based on a sequence identity threshold equal to or greater than 97% (thereafter referred to as 97% OTUs) using the clustering pipeline UPARSE (Edgar, 2013) in QIIME v.1.6.0, as described (Bates et al., 2014). Prokaryote phylotypes were classified according to their corresponding taxonomy by implementing the RDP classifier routine (Wang et al. 2007) in QIIME v. 1.6.0 (Caporaso et al. 2010) to interrogate the Greengenes 13.8 database (McDonald et al. 2012). All chloroplast and mitochondrial DNA sequences were removed. Finally, DNA sequence data were rarefied to a depth of 5,600 randomly selected reads per sample and two samples per treatment to achieve a standard number of sequencing reads across all samples.

Functional Potential of the microbiomes under different treatment conditions

Initially, the 16S rRNA amplicon sequence-based family-level taxonomic data were normalized with respect to a reference database containing the 16S copy numbers of microbial species. Individual microbes are considered to have contributed independently to the overall function/metabolism of a sample with their own enzyme pool. The enzyme abundance profiles for each individual taxa in a sample are represented by:

$$E = \sum_{i=1}^{n} Ec_i \; x \; Ab_i$$

Wherein,

E = Effective abundance value of an enzyme.

Ec_i = Enzyme Copy Number value in i^{th} taxon of a sample.

Ab_i = 16S and Sample Size Normalized Abundance Value (if chosen) of i^{th} taxon in the given sample.

n = Number of taxa expressing the Enzyme in the sample.

The enzyme abundance profile(s) are further used to compute the relative abundance of metabolic pathways at all three levels of the KEGG hierarchy. The following mathematical expression is used to calculate the pathway abundances for every taxon in a sample:

$$Pb = \sum_{i=1}^{n} E_i$$

Wherein,

Pb = Effective Abundance Value of the KEGG Pathway in b^{th} taxon of the sample

E_i = Effective abundance of i^{th} enzyme involved in the Pathway, as obtained in the Enzyme Abundance data for the b^{th} taxon

n = Number of enzymes (corresponding to the KEGG pathway) present in the taxon. The above steps are included in the iVikodak workflow (Nagpal et al. 2019) and has been utilised for inferring the functional profile of the microbial communities.

An unit variance scaling method followed by Singular Value Decomposition (SVD) were applied before performing the principal component analysis (PCA) on the functional contribution data. Hierarchical clustering of the heatmap starts with calculating all pairwise distances. Here, clustering distances are the Pearson correlation with the average distance of all possible pairs used for linking as described in ClustVis (Metsalu and Vilo 2015).

Real-time quantitative PCR

The abundances of the ROS responsive genes, *soxRS* and *oxyR*, for superoxide ion and hydrogen peroxide were determined using qPCR (QuantStudio 5 Real-Time PCR System). The total bacterial gene DNA was extracted from 1 mL samples using a PowerSoil DNA isolation kit (MoBio, Carlsbad, USA) as per the manufacturer's protocol. In brief, the qPCRs were performed using 5 µl of the Power SYBR® Green PCR master mix, 0.5 µl of the 10 µM forward and 10 µM reverse primers, and 2 µl of extracted gene DNA, made up to 10 µl with Gene

amplification was analysed by measuring fluorescence. The complete methodology is presented under Supplementary Information S1.2.

Protein extraction and identification

The enzymes for oxidative stress and central carbon metabolism (TCA and nitrogen cycle) were extracted by lysing cells in the dairy farm and municipal sludge cultures. One ml of the culture was pelleted at 16,000 xg for 5 min at 4°C and washed twice with 50 mM ammonium bicarbonate. The washed pellets were resuspended in 150 µl of 7M urea-thiourea buffer and sonicated for 15 s in three rounds on ice. The extracted proteins were separated from residual cellular material by centrifuging at 16,000 xg for 5 min. The proteins in the supernatant were quantified using the EZQ fluorescence protein assay (EZQ protein quantification kit) as per the manufacturer's protocol. Briefly, Trypsinization was performed on samples, and the proteins were recovered using HLB solid phase extraction cartridges. Finally, 30 µL of the generated tryptic peptides of the microbial proteins were injected into a SCIEX 6600 triple TOF mass spectrometer (AB Sciex, Australia). The proteins were identified by comparing the peptide sequences against UniProt database (Uniprot.org). The complete methodology is presented under Supplementary Information S1.3.

Metaproteome Data Analysis

Two separate pipelines for matching peptides were pursued to identify functions related to specific peptides. In the first pipeline, all 40 detected peptides were searched against the Uniprot database using the Peptide Search tool (https://www.uniprot.org/peptidesearch/). The data from Peptide Search was filtered for the 127 taxonomical families that were detected in the metagenome analysis. That is, any function associated with proteins from non-detected families was excluded. Peptides (GATVMISPYVMHR, WSEQGAAPASHLR) that were detected in experimental data but were excluded in the above analysis were manually added for subsequent analysis. In the second pipeline, the peptides were assigned to gene ontology (GO) terms using Unipept (Gurdeep Singh et al., 2019; Mesuere et al., 2015; Mesuere et al., 2018) through the proteomics Analysis tool (https://unipept.ugent.be/datasets). Default parameters were applied except the equating isoleucine and leucine option was unchecked. Any peptide sequence modified by the Unipept to search its database was reverted back to its original sequence in the final results to seamlessly intersect the results of both pipelines. Using the intersection table, the molecular functions (GO terms) of the microbial communities were analysed under different treatment conditions. First, the peptide intensities for the mapped GO

terms were summed and the average of the logs of the total intensities for biological replicates was calculated. After the data normalization with the HDO condition, a two-sided T-test was performed to identify the functions that changed significantly between different conditions. For the T-test, the null hypothesis that the averages of two independent samples are identical was assumed. To visualize the results of the analyses, scatterplots were utilized.

M-model simulations of archetypes

Archetypal analysis (AA) finds "archetypes" which are the points within the multivariate data set whose convex combination can well represent the data set (Cutler and Breiman 1994). It can be viewed as a dimension-reduction method such that each archetype refers to a distinct state of cell physiology. In this analysis, a dataset X can be approximated as

$$X \approx ZA,$$

where Z is the matrix of archetypes and A is a matrix of coefficients such that $A_{ij} \geq 0$ and $\Sigma_{j=1}^{p} A_{ij} = 1$ for p archetypes.

Likewise, Z can be constrained as

$$Z = XB$$

where B is the coefficient matrix such that $B_{ij} \geq 0$ and $\Sigma_{j=1}^{p} B_{ij} = 1$ for p archetypes such that Z is also constrained to be a convex combinations of the data points in X. The archetypal analysis was performed using *py_pcha* tool which is a python implementation of principal convex hull analysis (https://github.com/ulfaslak/py_pcha). The matrix used for the analyses was derived by performing simulations on a model of *Pseudomonas putida* KT2440 (*i*JN1463) constrained using targeted proteome data (Nogales et al. 2020). This model was used to study L-NE utilization in *Pseudomonas* species, which were the most abundant members of the microbiome.

We made two assumptions guided by the literature to modify this model. First, *P. putida* KT2440 is unable to catabolise several biogenic amines (Arcos et al. 2010), but L-NE degradation has been reported for several *Pseudomonas* species, so we added putative reactions for L-NE transport and metabolism for a related *Pseudomonas* strain, *Pseudomonas putida* U, to the model (Cuskey and Olsen 1988; Luengo and Olivera 2020). Second, as *Pseudomonas putida* cannot utilise methanol as the sole carbon source for growth (Hintermayer and Weuster-Botz 2017), we treated the reaction catalysed by formaldehyde dismutase as irreversible to

prevent methanol use for growth, consistent with the MetaCyc database (Caspi et al. 2020). We performed model simulations to optimise the growth rate under the following fluxes (shown in mmol gDW^{-1} hr^{-1}) for following substrates: 10 for acetate, 18 for oxygen, 100 for ammonium, and 1000 for methanol, sodium, phosphate, chloride, magnesium, calcium, potassium, iron, copper, sulphate, manganese, molybdenum, zinc, cobalt, nickel, water, and proton. Most fluxes were chosen based on the previous studies on M-models. Oxygen uptake rate constraint was approximated using another study (Gomez et al., 2005). The fluxes for acetate, ammonium, and methanol arbitrarily chosen based on their concentration in the experimental medium. The uptake fluxes for L-NE and dextrose for their respective medium were constrained at 6 mmol gDW^{-1} hr^{-1}.

Then, we performed parsimonious flux balance analysis (pFBA) (Lewis et al. 2010) using this medium for the HDO condition, i.e., without dextrose or L-NE in the medium. The proteins from the targeted proteome data were retrieved for *Pseudomonas putida*, and the reactions catalysed by those proteins were identified. Following this, the k_{effs} for each reaction-gene pair (associated with these proteins) was computed using the formula:

$$k_{eff} = (v_{pfba}/i) * N$$

where v_{pfba} is the flux computed by pFBA for the HDO condition, i is the protein intensity, and N is the number of reactions catalysed by a particular gene. Computed values of zero for k_{eff} were replaced with the lowest computed non-zero value. Subsequently, a target flux analysis was performed using HDO with dextrose or L-NE added at 6 mmol gDW^{-1} hr^{-1} for the reaction-gene pairs (specified above) using the formula:

$$v_t = k_{eff} * (i / N)$$

To obtain the target flux (v_t), which is influenced by proteome expression, for a specific reaction, the gene-reaction rules (e.g., linking gene *a* with gene *b* using AND or OR) were parsed such that for AND take the lower of the two genes and for OR take sum of the fluxes associated with these genes. Following the flux calculation, we performed a minimization of the sum of fluxes for these reactions (associated with proteins identified in proteomics) at fixed growth rates (μ) ranging from zero to the optimal growth rate (identified by FBA) using the following formula:

$$z = \sum(v - v_t)^2$$

where *z*, the sum of the square of errors, is the objective function and *v* is the flux obtained by simulating a particular condition.

We then performed another pFBA analysis at different growth rates (zero to FBA optimal growth rate) by bounding the fluxes of the reactions catalysed by the proteins identified in the proteome data using the fluxes predicted in the above minimisation procedure. These simulations provided the matrix containing rows (growth rates) and columns (reaction fluxes) that was then used in the subsequent archetypal analysis to identify representative archetypes of flux distribution (Cutler and Breiman 1994). For this analysis, 100 simulations were performed.

We chose two archetypes for the AA using the elbow method on the scree plot. These archetypes could explain >96% of the variance in both conditions (Figure S4). There were two other criteria for choosing the number of archetypes: 1) The growth rate in L-NE is higher than that in dextrose, and 2) the sum of squared error should be minimum as indicated by the elbow of the scree plot (Figure S5). In AA restricted by these points, we chose one archetype each at highest growth rates ~0.060 hr^{-1} and ~0.083 hr^{-1} for dextrose and L-NE growth conditions, respectively. These two archetypes (one for each condition) reflect the best approximation of the growth and proteomic assays. We next compare these two archetypes in the subsequent analyses and visualisation.

Simulated data analysis and visualisation

We used the Escher package (v. 1.7.3) in Python (v. 3.7.7) to visualise the maps of reaction fluxes normalised with the corresponding biomass flux (King et al., 2015). The normalization was performed to make the comparison between the proteome-constrained fluxes independent of the differences in growth rates between different conditions. For visualising pathways, we modified the maps created by the Escher online tool using Affinity Designer (v. 1.9.3). Genome-scale models typically contain information about subsystems, and we can use this knowledge to predict which subsystems are altered between two conditions. For the added pathways of L-NE transport and degradation, we assigned them the subsystem 'L-NE _Degradation' within the modified model (see ‘M-model simulations of archetypes’ method). We also made two modifications to the subsystems. 1) We removed LNE_Degradation subsystem as the pathway was assumed to be active in only for LNE utilization, and 2) Glycolysis and Gluconeogenesis were assigned to a new subsystem Glycolysis/Gluconeogenesis to avoid any confusion on the direction of the fluxes. Following

these changes, we identified five subsystems showing the most change by dividing the sum of the absolute difference in the normalised fluxes for two conditions by the number of reactions in the subsystem.

Results

Bacterial Growth and Shifts in microbial consortium

Preliminary experiments showed significant microbial growth in $5x10^{-5}$ M of L-NE, Dopamine and L-Dopa (Figure S1). Subsequent experiments were performed with different L-NE concentrations ($1x10^{-5}$ M, $5x10^{-5}$ M and $1x10^{-4}$ M) with the mixed farm (FS) and municipal (MS) cultures. Both cultures rapidly grew several-fold over 24 hours, increasing from 10^2 CFU mL^{-1} to 10^8 CFU mL^{-1} for $5x10^{-5}$ M L-NE but to a lower extent with $1x10^{-5}$ M (10^6 CFU mL^{-1}) and $1x10^{-4}$ M (10^7 CFU ml^{-1}) L-NE (Table S2). Although the dextrose samples contained ~10x carbon over the corresponding L-NE treatments, all L-NE concentrations showed higher cell growth over 8 and 24 h (Figure S1). The correlation graphs (Figure 1) show the bacterial abundances at the family level in municipal (MS) and dairy farm sludge (FS) treated with different concentrations ($1x10^{-5}$ M, $5x10^{-5}$ M, and $1x10^{-4}$ M) of L-NE, Dopamine ($5x10^{-5}$ M), L-Dopa ($5x10^{-5}$ M) and dextrose, where has been normalized by municipal sludge cultures treated at constant aeration (HDO) at 8 mg/L for 24 hours. As a control set, the ROS generating agents, 50 mM paraquat (PQ) and 50 mM hydrogen peroxide (H_2O_2) treated municipal sludge cultures were also normalized by HDO cultures and compared against $5x10^{-5}$ M dextrose. The reason behind choosing $5x10^{-5}$ M of Dopamine, L-Dopa, and dextrose is that maximum growth was observed in this concentration among all the studied samples.

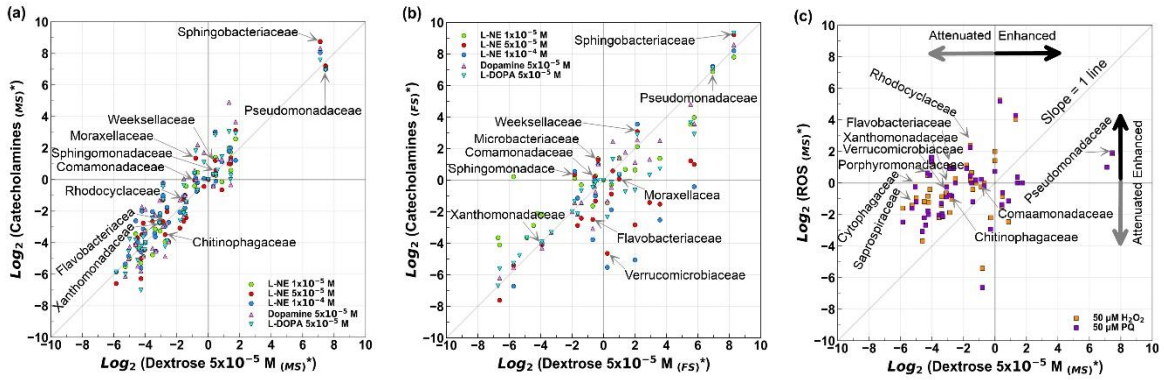

Figure 1: Correlation graphs comparing the effect of L-NE and ROS with dextrose on microbial abundances in the municipal (MS) and dairy farm (FS) sludge cultures. The top 10 abundant families in $5x10^{-5}$ M L-NE are labeled. Effects on microbial abundances in (a) and (b) respectively are shown for L-NE vs dextrose in municipal and dairy farm sludges, and in (c) for two ROS generating agents, 50 mM paraquat (PQ) and 50 mM hydrogen

peroxide (H_2O_2), vs dextrose. (Note: * represents scaling by dividing the abundances for the treatment with the corresponding values for $HDO_{(MS)}$).

Figure 1a showed the abundances of municipal sludge cultures treated with L-NE ($1x10^{-5}$ M, $5x10^{-5}$ M, and $1x10^{-4}$ M), Dopamine ($5x10^{-5}$ M), and L-Dopa ($5x10^{-5}$ M) against $5x10^{-5}$ M dextrose. The MS cultures treated with different concentrations of catecholamines showed a linear correlation pattern with the $5x10^{-5}$ M dextrose treated cultures indicating that the catecholamines have a similar effect on the microbial abundance as the $5x10^{-5}$ M dextrose cultures. *Pseudomonadaceae* is the most abundant family in all the conditions. However, other dominant families were present in a significantly much lower amount (0.004 to 0.113) than that of the *Pseudomonadaceae* (0.569 to 0.815). Out of the top 10, abundant families such as *Moraxellaceae*, *Sphingobacteriaceae*, *Weeksellaceae*, *Comamonadaceae*, *Flavobacteriaceae*, *Rhodocyclaceae*, *Sphingomonadaceae*, and *Verrucomicrobiaceae* were observed to preferably abundant in L-NE and other catecholamines than that of the Dextrose supplemented system.

Figure 1b, demonstrated that the dairy farm sludge (FS) cultures treated with catecholamine concentrations were similar to MS treatments against $5x10^{-5}$ M dextrose. However, the spread of the microbial families in the correlation plot showed significant diversification in the bacterial abundances as compared to the MS treatments, especially in $5x10^{-5}$ M and $1x10^{-4}$ M L-NE. *Pseudomonadaceae* remained the most dominant (0.548 to 0.692) microbial family in all the treatments involving FS samples. Other microbes lying within the top 10 abundant families exhibited low abundance ranging from 0.0007 to 0.147. The *Weeksellaceae*, *Comamonadaceae*, *Sphingomonadaceae*, and *Microbacteriaceae* had slightly preferential abundance in catecholamines whereas *Moraxellaceae*, *Flavobacteriaceae*, and *Verrucomicrobiaceae* appreciated being more abundant in dextrose treatment. Few families such as *Enterobacteriaceae*, *Lachnospiraceae*, *Peptostreptococcaceae*, *Rikenellaceae*, and *Microbacteriaceae* emerged within the top 10 families in the FS treatment. The speciation data indicates that the MS and FS samples are quite different in their source and influence altered microbial communities under similar perturbed conditions.

Furthermore, the $5x10^{-5}$ M Dextrose and the 50 uM paraquat (PQ) and 50 uM hydrogen peroxide (H_2O_2) treated municipal sludge cultures revealed significantly uncorrelated behaviour in the family level abundance profile (Figure 1c). The spread of the microbial population was more towards the ROS-treated samples than that of the dextrose treatment. The microbial abundances in the 50 μ M PQ and H_2O_2 treated municipal sludge cultures significantly deviated with respect to the $5x10^{-5}$ Dextrose cultures (Figure 1c). The effect of ROS was prominent as the families had a preferential growth in both H_2O_2 and PQ treatments

compared to the Dextrose supplemented system. Bacterial families such as *Rhodocyclaceae*, *Flavobacteriaceae*, *Chitinophagaceae*, *Comamonadaceae*, *Cytophagaceae*, and *Xanthomonadaceae* were the top five families in the ROS treated cultures. However, the abundance was very low (≤0.120) as a result of the stressed conditions.

Functional Profile and Bacterial Contribution Profile

The functional abundance profiles based on different pathways were inferred at the Pathway Exclusion Cut-off (PEC) of 80. The principal component analysis (PCA) was performed on the functional profiles of different treatment conditions in both MS and FS samples. Based on the contribution of different principal components the PC1 (72.4%) and PC2 (15.3%) were analysed further. The PCA indicated that the functional profiles in the Dextrose treatments had widespread distribution space in the scatterplot, indicating comparatively more variability than the catecholamines supplemented cultures (Figure 2). The catecholamines had less spread and overlapped with the Dextrose treated samples, signifying that the functional behaviour of the catecholamines is similar to the dextrose. On the other hand, the HDO (8 mg/L) and ROS (50µM H_2O_2 and 50µM PQ) treated systems exhibited similar behaviour which is quite different from both the catecholamines and dextrose treatments.

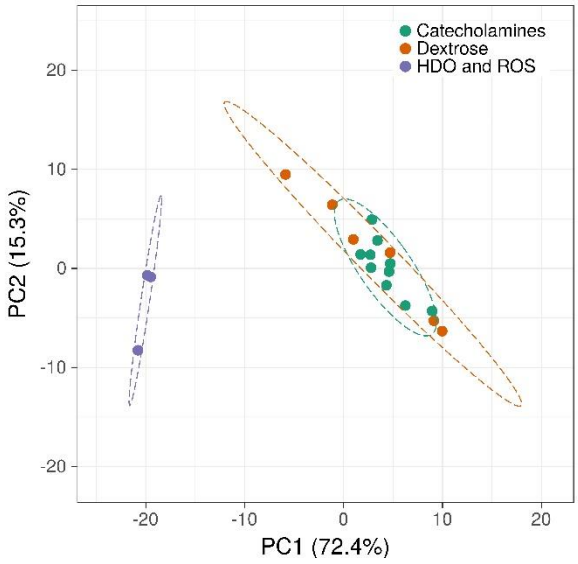

Figure 2. Principal component analysis (PCA) is based on the functional potential across different treatments showing that catecholamines exhibit a similar profile as the dextrose-treated samples. On the other hand, the distribution space of HDO and ROS behaviours are similar and quite different from both dextrose and catecholamines.

Furthermore, the $5x10^{-5}$ M Dextrose, L-NE, L-Dopa, and Dopamine treatments were clustered with the HDO and ROS systems, based on KEGG (L3) pathways and higher level (L2)

metabolism (Figure 3). As seen in the PCA plot, the HDO and ROS lie in a branch whereas the other treatments are clustered together in the other. Few pathways under carbohydrate metabolism such as Fructose and mannose metabolism, Galactose metabolism, Amino sugar and nucleotide sugar metabolism, Pentose and glucuronate interconversions were comparatively active in HDO and ROS treated systems than that of the Catecholamines and Dextrose treated samples. Other pathways involved in carbohydrate metabolism, such as the Citrate cycle TCA cycle, Glyoxylate and dicarboxylate metabolism, Propanoate metabolism, C5, Branched dibasic acid metabolism, Pyruvate metabolism, Glycolysis Gluconeogenesis and Pentose phosphate pathway were observed to be upregulated in both the dextrose and catecholamines, especially 5x10-5 L-NE (FS), Dextrose (MS). The energy metabolism involving the Oxidative phosphorylation, Nitrogen metabolism, and Sulfur metabolism also had a right metabolic shift from HDO base control and upregulated in different catecholamines and dextrose supplemented systems. Similar upregulation was also observed in the case of amino-acid metabolism under catecholamine treatments, except for the D-alanine, D-Arginine, and D-ornithine metabolism, Selenocompound metabolism, which were upregulated in the ROS treatments. Interestingly, the glutathione metabolism, which is generally activated during ROS stress conditions, was found to be active in catecholamines and dextrose samples only. Also, along with the fatty acid metabolism, the Lipopolysaccharide biosynthesis and Peptidoglycan biosynthesis were upregulated supporting the growth under different catecholamine treatments. The Glycosaminoglycan and other glycan degradation were significant in the ROS stress conditions.

In terms of genetic information processing, the purine metabolism was upregulated in L-NE and Dextrose treatment whereas the pyrimidine expressions were higher in ROS and HDO conditions. The DNA replication and mismatch repair were also found to be significantly high in these conditions. Furthermore, the quorum sensing capability under the dextrose and catecholamines were higher than the ROS treatments as well.

The functional contribution of the microbes revealed a major shift in the population in different treatment conditions compared to the controls. In the case of the MS samples, the top five contributors to the overall functions were *Chitinophagaceae*, *Saprospiraceae*, *Rhodobacteraceae*, *Cytophagaceae*, and *Comamonadaceae* in HDO treatment, which was shifted to *Pseudomonadaceae*, *Sphingobacteriaceae*, *Moraxellaceae*, *Comamonadaceae*, and *Rhodocyclaceae* in the $5x10^{-5}$ M L-NE, whereas *Chitinophagaceae* came up instead of *Rhodocyclaceae* in the $5x10^{-5}$ M Dextrose (Figure S2). Interestingly, in all the L-NE, Dextrose,

Dopamine, and L-Dopa treatments the metabolic capabilities were dominated by *Pseudomonadaceae* (Figure S2). A similar trend was observed in the FS also.

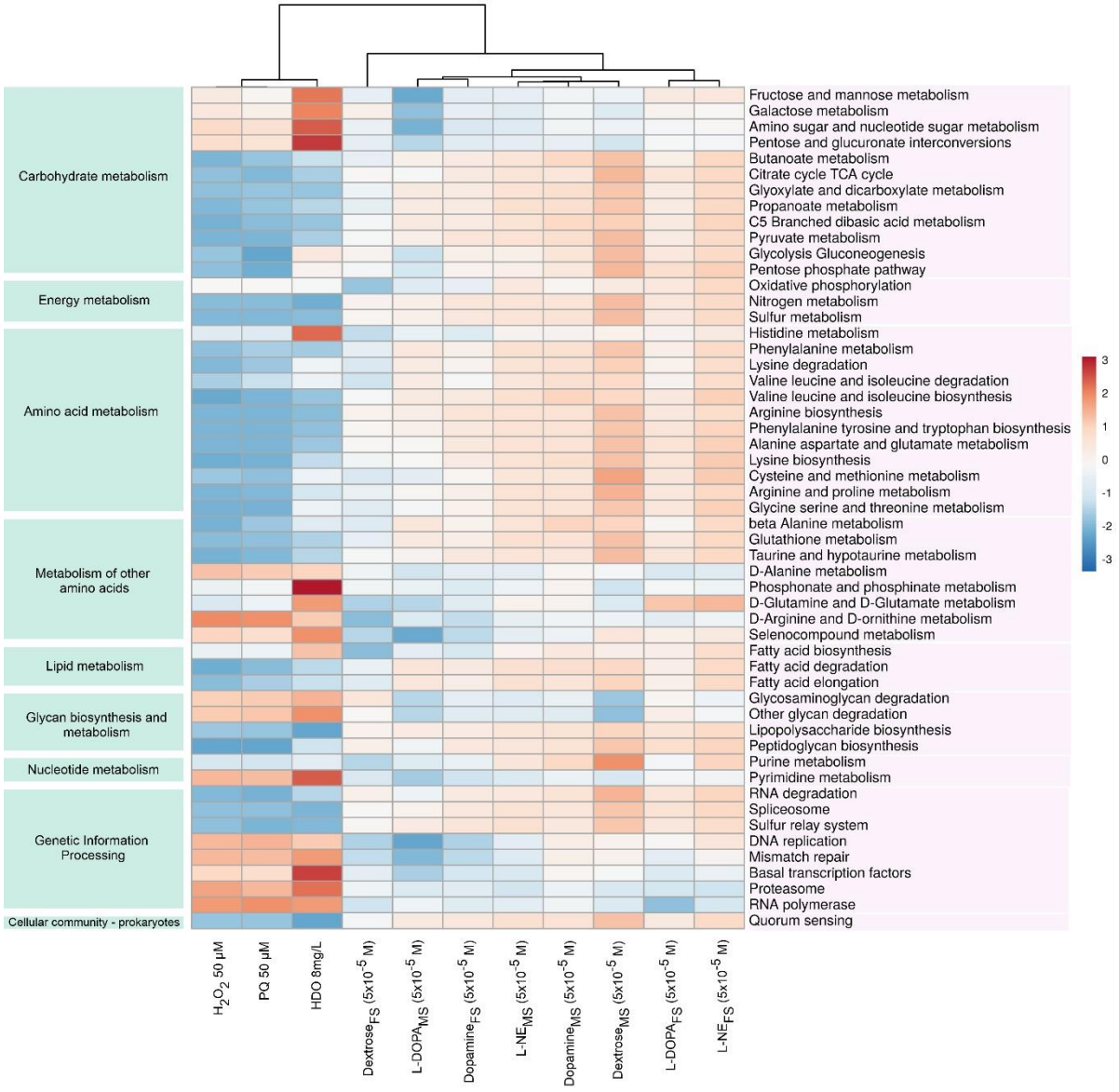

Figure 3. The functional potential of the microbial communities is shown under different treatments. The samples are clustered using correlation distance and average linkage. Based on the KEGG database, the pathways (L2) are groups based on their higher-level metabolic functions (L3).

Abundance of ROS genes

The abundances of the *soxRS* and *oxyR* oxidative stress genes, using the 16S house-keeping gene as a reference, are shown in Figure S3 for the different treatments. The higher *soxRS* and *oxyR* genes abundances show that 1×10^{-5} M, 5×10^{-5} M and 1×10^{-4} M L-NE caused ROS formation within microbial cells (Figure S3). The HDO and dextrose treatments show a low abundance of the stress genes. The 50 µM PQ increased the s*oxRS* gene abundance, and both

50 μM PQ and 50 μM H_2O_2 increased the *oxyR* abundance. However, 50 μM PQ caused a lesser change than 50 μM H_2O_2. The *soxRS* gene abundance was low in all L-NE treatments. The *oxyR* abundance varied greatly for different L-NE concentrations, with $5x10^{-5}$ M inducing the highest response, indicating that most ROS formation in the dairy farm and municipal cultures occurred for this condition. The similarity in *oxyR* abundances for 50 μM H_2O_2 and $5x10^{-5}$ M L-NE suggests that these treatments caused similar levels of oxidative stress in dairy farm and municipal sludge cultures.

Functional analysis of targeted proteins

Figure 4 presents the gene ontology (GO) categories using peptides from the target proteomics analysis of the 50 μM PQ and 50 μM H_2O_2 from municipal sludge cultures and 5×10^{-5} M dextrose, and 5×10^{-5} M L-NE from dairy farm sludge treatments. The L-NE treatment generates response that is considerably different to the dextrose and H_2O_2 or PQ treatments. Compared to dextrose, L-NE upregulated most of the oxidative stress associated functions except for monooxygenase activity (GO:0004497, 6 peptides) and ammonia monooxygenase activity (GO:0018597, 2 peptides) (Figure 4a). Proteins with ammonia monooxygenase activity catalyse the conversion of ammonia to hydroxylamine. However, L-NE upregulates glutamate-ammonia ligase activity (GO:0004356, 3 peptides), indicating a shift in the nitrogen flux in the community towards glutamine production. In terms of nitrogen metabolism, L-NE upregulated the functions related to anaerobic respiration (nitrous oxide reductase (GO:0050304, 1 peptide) and nitrate reductase (GO:0008940, 8 peptides)). Additionally, L-NE induces ROS detoxification by upregulating thioredoxin-disulfide reductase activity, thioredoxin peroxidase activity, catalase activity, peroxidase activity, and oxidoreductase activity.

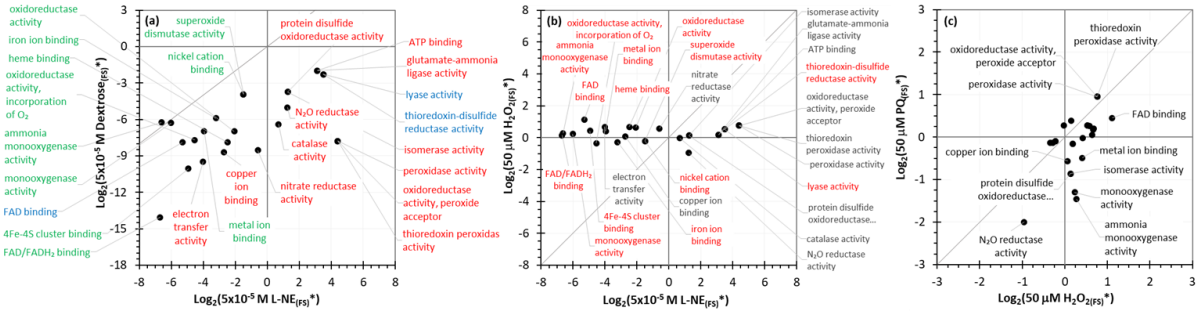

Figure 4. Alterations to protein functions caused by different organic carbon substrate and oxidative stress conditions. Plots show: (a) 5×10^{-5} M Dextrose vs 5×10^{-5} M L-NE, (b) 50 mM H_2O_2 vs 5×10^{-5} M L-NE, and (c) 50 mM PQ vs 50 mM H_2O_2. Different colour fonts identify rescaled GO terms with fold change ≥ 1 at $p < 0.05$, determined by t-test: red, significantly expressed in L-NE; blue, significantly expressed in dextrose; green,

significantly expressed in dextrose and L-NE; and black, no significant expression. (Note: * represents scaling by dividing the abundances for the treatment with the corresponding values for $HDO_{(MS)}$).

Compared to 50 μM H_2O_2 (Figure 4b), L-NE upregulates GO categories such as ATP binding, oxidoreductase, peroxidase, lyase, isomerase, glutamate-ammonia ligase and N_2O reductase activities. In particular, the thioredoxin-disulfide reductase activity (GO:0004791, 1 peptide) and thioredoxin peroxidase activity (GO:0008379, 1 peptide), involved in the redox balancing of thioredoxins and H_2O_2 detoxification, are significantly upregulated. The downregulated functions include copper ion, nickel cation and iron ion binding, electron transfer, 4Fe-4S cluster and FAD/$FADH_2$ binding, and oxidoreductase, ammonia monooxygenase, heme binding activities. L-NE and H_2O_2 showed similar levels of superoxide dismutase and catalase activities.

PQ and H_2O_2 treatments showed a strong correlation (Figure 4c) with few deviations, such as the ammonia monooxygenase (GO:0018597, 2 peptides) and nitrous oxide reductase (GO:0050304, 1 peptide) activity. Compared to PQ, H_2O_2 upregulated the electron transfer protein (FAD binding activity). Additionally, the PQ and H_2O_2 responses were concentrated around (0,0) origin, indicating a similarity in function under these conditions to the HDO treatment.

M-model prediction of metabolic activities

Pseudomonadaceae was the dominant family under both catecholamines and dextrose conditions (Figure 1) and *Pseudomonas* was among the most dominant genera. A flux balance analysis performed using the proteome-constrained genome-scale model of *Pseudomonas putida* KT2440, a model *Pseudomonas* species showed a variation in the regulation of different metabolic mechanisms such as oxidative phosphorylation, gluconeogenesis, glycolysis and glutamate metabolism between L-NE and dextrose treated cultures. The flux map in Figure 5 shows a significant shift in the oxygen consumption in L-NE cultures compared to dextrose possibly due to higher terminal oxidase activity leading to more ATP production. The addition of lower TCA cycle intermediates to stationary phase cells leads to higher oxygen consumption and proton motive force (Meylan et al., 2017). Additionally, *Pseudomonas* growth rate is higher in media supplemented with TCA intermediates such as succinate compared to dextrose (Tiwari and Campbell, 1969; Nikel et al., 2014; Nikel et al., 2015). Although L-NE may not be an energetically favourable carbon source, by providing TCA cycle intermediates it can enhance microbial growth on other substrates in the complex media (Meylan et al., 2017).

Other factors such as autoinducers could also contribute to increasing the growth rate by L-NE, but metabolic models are unable to capture such aspects. Compared to dextrose, L-NE induces a stronger oxidative stress mitigation response in the community. For instance, the glutathione-based peroxidase activity is considerably higher in L-NE cultures than in dextrose cultures. Furthermore, thioredoxin-based oxidative stress mitigation was also elevated in L-NE cultures. The model predicted changes to sulphur metabolism by L-NE, which are consistent with alterations to proteins of the sulphur metabolism by H_2O_2 and PQ induced oxidative stress in *Pseudomonas* strains (Palma et al., 2004; Hare et al., 2011; Yeom et al., 2012; Bojanovicˇ et al., 2017). The use of sulfur-containing redox metabolites (e.g., thioredoxin and glutathione) correlates with the enhancement of the sulphur metabolism in *Pseudomonas* in L-NE condition. Simulations also show that L-NE affects nitrogen metabolism through the glutamate pathway, consistent with the targeted proteomics data.

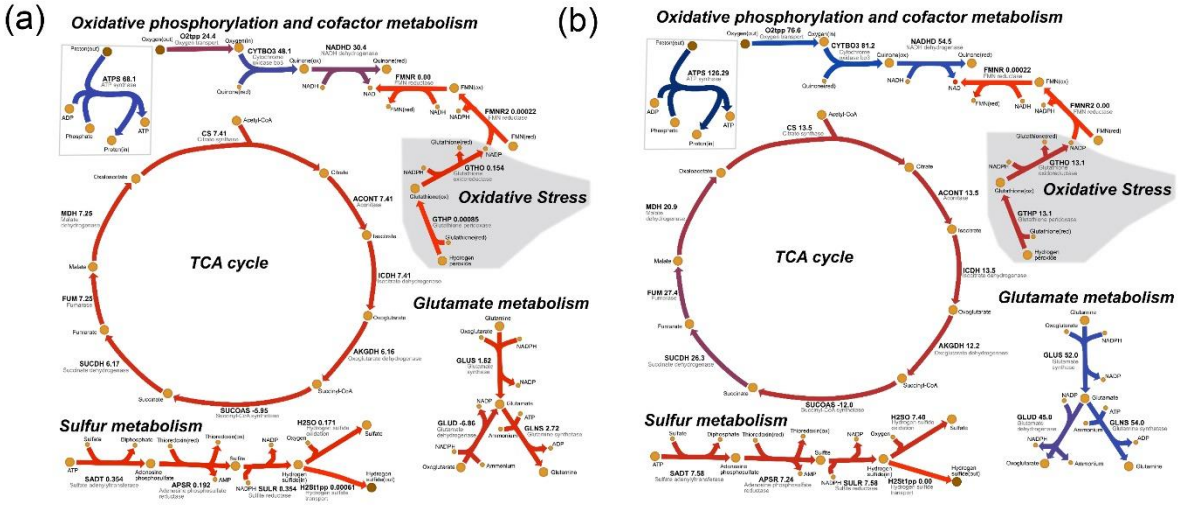

Figure 5. Pathway maps showing normalised fluxes for (a) L-NE and (b) dextrose treatments. Darker shades of different colours indicate higher values: lower fluxes are coloured red, mid-range fluxes are coloured blue, and the highest fluxes are coloured purple. The higher growth rate in the L-NE treatment compared to dextrose result from increased O2 consumption, which shifts the fluxes towards greater terminal oxidase and ATP synthase activity. L-NE additionally reprograms the cofactor metabolism, sulphur metabolism, and thioredoxin-based and glutathione-based oxidative stress mitigation strategies. In the model, reaction GLNS and FMN reductase reactions are split into two, and the map shows only one of these fluxes.

Discussion

Microbial speciation diversification and growth

The bacterial community structure and composition within or between activated sludge systems have been widely investigated. Bacterial community dynamics are thought to be influenced by

changing environmental or operational variables. However, understanding the temporal dynamics of microbial community is one of the ways to correlate environmental or operational variable with bacterial community and functions to improve the treatment performances and predicting responses to unexpected environmental shifts. L-norepinephrine is a well-known stimulant to enhance the low biomass growth *in vivo* (Freestone et al. 1999). Our results show that L-NE enhances the bacterial growth in farm (FS) and municipal sludge (MS). The enhancement of growth may be tied in part to an individual bacterium's ability to utilise neurochemical present in the vicinity. Moreover, *Pseudomonadaceae* was the most dominant family in both the FS and MS cultures for the Dextrose or L-NE treatments. Also, the family abundances for these treatments show strong correlation, indicating that the catecholamine and Dextrose treatments affect the FS and MS communities in a similar manner. In contrast, the application of ROS dramatically alters the microbial community composition with the family abundances showing no correlation with the Dextrose treatment. Though the MS cultures treated with different concentrations of catecholamines exhibited a linear correlation pattern with the $5x10^{-5}$ M dextrose treated cultures, some differences in the $5x10^{-5}$ M and $1x10^{-4}$ M L-NE were observed in the FS cultures. It indicted that the source environment could also influence the microbial community composition. The L-NE and dextrose treatments showed a shift in the bacterial community composition compared to original farm and municipal sludge cultures. The bacterial community composition might be similar between control (dextrose) and L-NE treated groups, but they vary in their abundances. Likewise, microbes that have a better ability to adapt to ROS stress are more likely to survive. The microbes surviving ROS stress are *Pseudomonadaceae, Moraxellaceae, Rhodocyclaceae, Xanthomonadaceae, Halomonadaceae* and *Methylophilaceae* which is in accord with the previous studies (Svenningsen *et al.*, 2015; Barra Caracciolo, Topp and Grenni, 2015). Despite the formation of H_2O_2 in L-NE treatments, the microbial abundances differed for L-NE and exogenous ROS (H_2O_2 and PQ) applications (Figure 1). In contrast, while the dextrose treatments showed a slight or no increase in the *oxyR* gene abundance, indicative of minimal H_2O_2 formation, the microbial abundances for L-NE and dextrose were similar. The similarity with dextrose suggests that the ROS stress induced by L-NE, even at the elevated ~50 μM H_2O_2 level, was dominated by changes associated with growth substrates like dextrose.

Functional Potential of the Microbial communities

The PCA analysis shows that the H_2O_2 and PQ treatments affect the microbial community functions similarly, while the effect of HDO is closer to H_2O_2 and PQ compared to the Dextrose

and catecholamine treatments. The addition of Dextrose or catecholamines causes a major shift in the community behaviour; the addition of catecholamines to FS and MS microbial communities causes a similar effect as the provision of Dextrose. The microbial families selected by the HDO condition showed the largest function potentials for sugar metabolism (fructose and mannose metabolism, galactose metabolism, amino sugar and nucleotide sugar metabolism and pentose and glutamate interconversions). This reflects low sugar availability and that microbes that are able to sequester sugars thrive under this condition. The HOD treatment also shows higher potential for fatty acid biosynthesis, indicating a combination of processes supporting growth but also coping with stress. The families selected by HDO, H_2O_2 and PQ show high function potential for pyrimidine as well. Nucleotide metabolism is a critical pathway that generates purine and pyrimidine molecules for DNA replication, RNA synthesis, and cellular bioenergetics. Cells with phenotypes showing resistance to DNA damage and cell death exhibit increased expressions of PyM genes (Siddiqui and Ceppi 2020). Thus, the selected families were better able to resist the DNA damage by ROS created by these conditions. The absence of higher pyrimidine metabolism for L-NE indicates that DNA damage by ROS formed under this condition was not a dominant selection criteria for the dominant species.

Adding dextrose shifts the selection criteria towards growth over stress mitigation seen in the H_2O_2 and PQ. The HDO condition shows microbial attempts to grow under stress. So we see a combination of stress mitigation and growth by sequestering organic carbon and fatty acid biosynthesis. As enough carbon source are present in both L-NE and dextrose, the core carbohydrate metabolic pathways such as the Citrate cycle TCA cycle, Pyruvate metabolism, Glycolysis Gluconeogenesis and Pentose phosphate pathway were observed to be upregulated. The increased energy metabolism (Oxidative phosphorylation, Nitrogen metabolism, and Sulfur metabolism), lipid metabolism (fatty acid biosynthesis), amino-acid metabolism and glycan biosynthesis and metabolism (Lipopolysaccharide biosynthesis and Peptidoglycan biosynthesis) were indicative of enhanced growth in these systems compared to the HDO and ROS treatments. Interestingly, the glutathione pathway which is associated with the ROS stress mitigation, was upregulated under Dextrose and catecholamines instead of the ROS supplemented systems. The lack of carbon source in the ROS treated systems didn't significantly upregulate the Citrate cycle TCA cycle enzymes, thereby leading to less expression of the glutathione pathway. Some of the dextrose and catecholamine treatments show increased capacity for purine metabolism in the abundant families. Purines are key

components of cellular energy systems (e.g., ATP, NAD), and, along with pyrimidines, RNA and DNA production and the increase in purine metabolism reflects the ability of these families to generate more ATP and NAD. These dextrose and catecholamine treatments showed higher function potential for a range of biosynthesis pathways to enable the high growth observed under these conditions.

While the most abundant families make the highest contribution to various metabolisms, the absolute contribution by the individual families varies under different conditions. For conditions stimulating growth, *Pseudomonadaceae* dominates. However, in comparison to dextrose, L-NE treatments promote contributions by more families to the various metabolisms. The application of stress in the H_2O_2 and HDO treatments decreases the absolute contributions to metabolism and increased the number of families that make relatively significant contributions to the various metabolisms. Thus stress appears to increase interdependence between the different families while growth decreases this interdependence and allows a smaller number of families to thrive in the population.

Oxidative stress response

The overproduction of intracellular ROS in the L-NE cultures can be elucidated by different ways: constant aeration, and the oxidative deamination of L-NE by oxidase in the presence of oxygen to form hydrogen peroxide (Buhlman, 2016; Lyte & Freestone, 2010; Neri et al., 2007). The L-NE treatments led to the generation of ROS under aerobic conditions and might contribute to the species selection due to the toxic effects of ROS along with their role as messaging molecules (Dickinson & Chang, 2011). Microbes control the $O_2^{-\cdot}$ and H_2O_2 levels by the activation of *soxRS* and *oxyR* genes, which regulates the expression of ROS scavenging enzymes such as superoxide dismutase (SODs), catalase and thioredoxin reductase (Imlay, 2013). The higher expression of superoxide dismutase and catalase-peroxidase activities in L-NE cultures compared to dextrose suggests the activation of *soxRS* and *oxyR* genes due to the formation of larger amounts of $O_2^{-\cdot}$ & H_2O_2. The production of ammonia monooxygenase, laccase, cytochrome c, cytochrome P450 and oxidoreductases were also higher in L-NE treatments.

Functional changes by proteome analysis

The proteomics analysis of the mixed culture pool from farm sludge revealed proteins related to several cellular functions such as metabolism (nitrogen metabolism, oxidative phosphorylation), genetic information processing, and environmental information processing.

Additionally, a functional analysis of targeted proteins showed significant upregulation of oxidative stress related activities such as catalase-peroxidase activity, thioredoxin disulphide reductase activity by $5x10^{-5}$ M L-NE cultures compared to $5x10^{-5}$ M dextrose (Figure 4). A significant upregulation of glutamine-ammonia ligase activity in the L-NE cultures demonstrates alteration of cellular nitrogen metabolism via flux redirection towards glutamate/glutamine synthesis. Compared to exogenous 50 μM PQ and 50 μM H_2O_2, $5x10^{-5}$ M L-NE significantly upregulated thioredoxin-based oxidative stress detoxification. Thioredoxin reductases are involved in the redox balancing of thioredoxins that repair disulfide bonds (formed due to oxidative stress) to maintain the catalytic activity of enzymes (Arts et al., 2016). Thioredoxin peroxidase is also associated with enzymes that detoxify H_2O_2 using thioredoxin as a reducing agent (Somprasong et al., 2012). Compared to $5x10^{-5}$ M L-NE, 50 μM PQ and 50 μM H_2O_2 led to higher expression of superoxide dismutase, which catalyses superoxide ($O_2^{\cdot-}$) dismutation into O_2 and H_2O_2. Microbes control the $O_2^{\cdot-}$ and H_2O_2 levels by the activation of *soxRS* and *oxyR* genes, which regulate the expression of ROS scavenging enzymes such as superoxide dismutase (SODs), catalase and thioredoxin reductase (Imlay, 2013). The higher expression of catalase-peroxidase and thioredoxin reductase activities in L-NE cultures compared to H_2O_2 suggests the activation of *oxyR* genes due to the formation of larger amounts of H_2O_2. However, the microbial proteomic activities differ when treated with L-NE and dextrose. The significant upregulation of anti-oxidative stress activities such as catalase activity, thioredoxin and superoxide dismutase activity in L-NE treated farm sludge cultures at $5x10^{-5}$ M compared to dextrose treatments shows the fact that L-NE generates enough intracellular ROS stress to activate the *soxRS* and *oxyR* genes and regulate their proteomic expressions (Figure S3). L-NE treatment also leads to higher expression of nitrogen reductase and glutamate-ammonia ligase activity. Hence, this knowledge can provide opportunities for the manipulation of community nitrogen metabolism for resource recovery process. Furthermore, the higher expression of the oxidoreductases, monooxygenases, copper ion binding laccases and heme binding cytochromes in L-NE treated cultures compared to dextrose cultures indicates the potential of bacterial families such as *Rhodocyclaceae, Xanthomonadacea* and *Pseudomonadaceae* in the removal of organic micropollutants.

Thus, this study indicates the regulation of ROS mitigation activities in L-NE cultures were different from those in dextrose, PQ and H_2O_2 treatments. However, the comparison of ROS treated (PQ and H_2O_2) control cultures showed different activities with regulation of nitrogen metabolic activities. It demonstrated that the ROS treated cultures might show the mixotrophic

effect. It can also be postulated that the *in situ* metabolic activities of many biogeochemically critical microbial populations (involved in the cycling of C and N and other elements) may be regulated by adjacent species that produce enzymes able to detoxify toxic reactive oxygen species, particularly H_2O_2 (Kim et al., 2016).

Proteome-constrained flux balance analysis suggests ATP production is upregulated in L-NE because of shift in cofactor recycling

A flux balance analysis (FBA) by applying protein constraints on the genome-scale model of *Pseudomonas putida* KT2440 (Nogales et al., 2020) was performed in this study to investigate the metabolic reprogramming in L-NE treatment when compared to dextrose treatment. A custom metaproteome-based flux scaling pipeline was developed to apply the protein constraints followed by archetypal analyses to identify the archetypes to best explain the differences between the two treatments. The custom method for integrating targeted proteome data expanded the findings of the targeted proteomics to global metabolic pathways, and provided deeper insights into the metabolic state of *Pseudomonas* in media supplemented with L-NE. The analysis revealed that the addition of L-NE alters various biochemical systems, such as oxidative phosphorylation, gluconeogenesis, glycolysis and glutamate metabolism (Figure 5). Figure 5 shows Escher maps to visualise the flux redistribution in key pathways of the dextrose and L-NE treatments. L-NE upregulates the TCA cycle and the associated oxidative phosphorylation pathways. Higher fluxes through the TCA cycle and cofactor pathways, including terminal oxidase reactions, likely lead to more oxygen consumption and drive up the ATP synthase reaction. Likewise, the L-NE degradation pathway links to the regeneration of NADH cofactor, which influences the recycling of FMN, ubiquinone and NADP cofactors. In agreement with the proteomic data, compared to dextrose, the simulations predict that L-NE alters the nitrogen (glutamate/glutamine synthesis) and carbon-associated (TCA cycle) pathways. The model expands on the proteomic results by indicating that *Pseudomonas* primarily uses glutathione-based elimination of oxidative stress in the simulated conditions. This process most likely is associated with the reprogramming of sulphur metabolism (Figure 6). Using the metabolic model, the knowledge of metabolic reprogramming by L-NE might be applied on the microbial community to increase the rate of resource recovery.

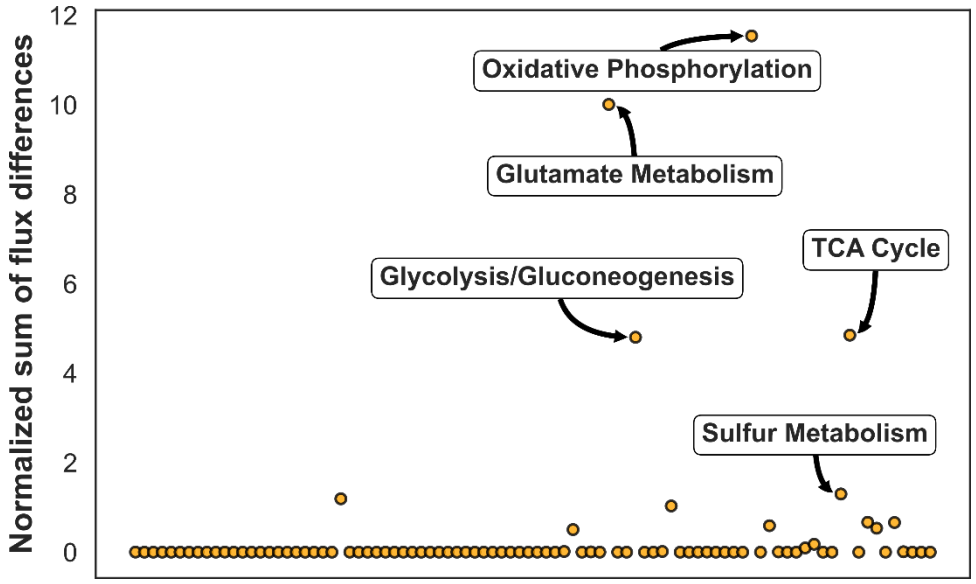

Figure 6. A scatterplot of the predicted normalized fluxes. To determine the subsystems that were differentially changed between dextrose and L-NE conditions, the absolute flux values were normalized and the difference was computed between L-NE and dextrose. Following this, the absolute difference was summed up for each subsystem. The top five subsystems that were altered between the two conditions are shown in the figure.

This study demonstrated that L-NE treatment showed the diversification of the mixed microbial cultures by significant formation of ROS by enzymatic oxidation as well as alteration of nitrogen assimilation and sulphur metabolic activities in L-NE cultures compared to dextrose and PQ/H_2O_2 treated cultures. The generation of more energy producing molecules and increased catalase flux in L-NE cultures cause enhanced bacterial growth. The comparison of different levels of L-NE and with ROS ions and dextrose showed the variability in the microbial species abundance. The abundance of pathogenic bacteria at lower concentrations of L-NE indicated that L-NE at less than 1×10^{-5} M concentration can lead to the proliferation of the antibiotic resistant species. The cultures treated with concentration more than 5×10^{-5} M shifts the survival of the species that assimilate more carbon and nitrogen to enhance the biological activities in wastewater treatment systems such as nitrification and denitrification processes.

M-model predicting the expression of different metabolic activities

A flux balance analysis performed on *Pseudomonas putida* KT2440 showed a variation in the regulation of different molecular metabolic mechanisms such as oxidative phosphorylation, gluconeogenesis, glycolysis and glutamate metabolism in L-NE and dextrose treated cultures. *P. putida* KT2440 naturally does not possess the machinery to catabolize several biogenic amines (Arcos et al., 2010). The core *Pseudomonas* putida model has been demonstrated to contain the same gene content as in at least 95% of other *Pseudomonas putida* reconstructions

(Nogales et al., 2020). Since the computational analyses were performed assuming the genome-scale model is representative of the community *Pseudomonas* strains, the L-NE degradation pathway of the related *Pseudomonas* strain, *Pseudomonas putida* U was added to the model in order to study the effect of L-NE on the *Pseudomonas* strains of the microbial community. Another consideration while constraining the model was that the proteomic data were available for 24-hour cultures at which point the growth rates were very low (~0.01-0.04). To make sure the proteome-constrained fluxes were comparable between L-NE and dextrose cultures, the fluxes were normalized by the respective growth rates. Further, to remove the effect of methanol utilization and to focus on the effect of L-NE and dextrose, reaction catalyzed by formaldehyde dehydrogenase was made irreversible.

Through the flux map, it can be predicted that a significant shift in the oxygen consumption occurs in L-NE cultures compared to dextrose due to higher terminal oxidase activity leading to more ATP production. It has been demonstrated that for stationary phase cells, the addition of lower TCA cycle intermediates leads to higher oxygen consumption and proton motive force (Meylan et al., 2017). Additionally, studies have revealed that *Pseudomonas* grows at a higher rate on media supplemented with TCA intermediates such as succinate than on glucose media (Tiwari and Campbell, 1969; Nikel et al., 2014; Nikel et al., 2015). The process of higher oxygen consumption, according to the model, is associated with higher fluxes through multiple cofactor regeneration pathways. It should be noted that L-NE might not be an energetically favourable carbon source, but because it provides TCA cycle intermediates, it could enhance the ability of organisms to grow on other substrates within the complex media provided. Likewise, other factors including autoinducers could also partly contribute to the higher growth rate in L-NE, but such insights cannot be gathered using metabolic models.

The mitigation strategies for oxidative stress caused by hydrogen peroxide or paraquat are also different to those of L-NE which are primarily through glutathione- and thioredoxin-based reactions (Palma et al., 2004; Hare et al., 2011; Yeom et al., 2012; Bojanovicˇ et al., 2017). The catalase flux is higher in L-NE compared to that in dextrose but compared to the fluxes of other oxidative stress-related reactions, catalase flux is negligible. The use of these redox metabolites (thioredoxin and glutathione) correlates with the changes to the sulfur metabolism in *Pseudomonas*. Alterations to the genes/proteins related to sulfur metabolism during oxidative stress has also been observed in the case of supplementation of media with hydrogen peroxide and paraquat in *Pseudomonas* strains (Palma et al., 2004; Hare et al., 2011; Yeom et al., 2012; Bojanovicˇ et al., 2017). Therefore, sulfur metabolism likely is closely associated

with oxidative stress response caused by L-NE and other ROS agents in addition to nitrogen metabolism. The effects of L-NE on nitrogen metabolism through the glutamine pathway was also predicted by the simulations, and these results are also supported by the targeted proteomic data.

Our custom method for integrating targeted proteome data has expanded the findings of targeted proteomics to global metabolic pathways, and provided deeper insights into the metabolic state of *Pseudomonas* in media supplemented with L-NE. By using proteome-constrained M-model, we can predict that L-NE not only acts as an oxidative stress inducer, but also a carbon source which directly feeds into the TCA cycle; characterization of the strengths of both responses is beyond the scope of this study. Nonetheless, this result likely explains the targeted experimental data which show that L-NE response is intermediate between dextrose and PQ/H_2O_2 responses.

Declaration of Competing Interest

All the authors declare that they have no conflict of interest.

Acknowledgment

This project was partially funded by an award from the Royal Society of New Zealand's Marsden Fund (Contract Number: MFP-UOA2018). The authors thank the Gavin Lear group for performing the microbial taxonomic analyses.

References

Arcos, Mario, Elías R. Olivera, Sagrario Arias, Germán Naharro, and José M. Luengo. 2010. "The 3,4-Dihydroxyphenylacetic Acid Catabolon, a Catabolic Unit for Degradation of Biogenic Amines Tyramine and Dopamine in Pseudomonas Putida U." *Environmental Microbiology*. doi: 10.1111/j.1462-2920.2010.02233.x.

Bansal, Tarun, Derek Englert, Jintae Lee, Manjunath Hegde, Thomas K. Wood, and Arul Jayaraman. 2007. "Differential Effects of Epinephrine, Norepinephrine, and Indole on Escherichia Coli O157:H7 Chemotaxis, Colonization, and Gene Expression." *Infection and Immunity*. doi: 10.1128/IAI.00630-07.

Belay, Tesfaye, Hernan Aviles, Monique Vance, Kimberly Fountain, and Gerald Sonnenfeld. 2003. "Catecholamines and in Vitro Growth of Pathogenic Bacteria: Enhancement of Growth Varies Greatly among Bacterial Species." *Life Sciences*. doi: 10.1016/S0024-3205(03)00472-7.

Bonavita, Raffaella, and Mikko O. Laukkanen. 2021. "Common Signal Transduction Molecules Activated by Bacterial Entry into a Host Cell and by Reactive Oxygen Species." *Antioxidants and Redox Signaling*.

Burton, Claire L., Siri Ram Chhabra, Simon Swift, Tom J. Baldwin, Helen Withers, Stephen J. Hill, and Paul Williams. 2002. "The Growth Response of Escherichia Coli to Neurotransmitters and Related Catecholamine Drugs Requires a Functional Enterobactin Biosynthesis and Uptake System." *Infection and Immunity*. doi: 10.1128/IAI.70.11.5913-5923.2002.

Caporaso, J. Gregory, Justin Kuczynski, Jesse Stombaugh, Kyle Bittinger, Frederic D. Bushman, Elizabeth K. Costello, Noah Fierer, Antonio Gonzalez Pẽa, Julia K. Goodrich, Jeffrey I. Gordon, Gavin A. Huttley, Scott T. Kelley, Dan Knights, Jeremy E. Koenig, Ruth E. Ley, Catherine A. Lozupone, Daniel McDonald, Brian D. Muegge, Meg Pirrung, Jens Reeder, Joel R. Sevinsky, Peter J. Turnbaugh, William A. Walters, Jeremy Widmann, Tanya Yatsunenko, Jesse Zaneveld, and Rob Knight. 2010. "QIIME Allows Analysis of High-Throughput Community Sequencing Data." *Nature Methods*.

Caspi, Ron, Richard Billington, Ingrid M. Keseler, Anamika Kothari, Markus Krummenacker, Peter E. Midford, Wai Kit Ong, Suzanne Paley, Pallavi Subhraveti, and Peter D. Karp. 2020. "The MetaCyc Database of Metabolic Pathways and Enzymes-a 2019 Update." *Nucleic Acids Research*. doi: 10.1093/nar/gkz862.

Chen, Chunsheng, David R. Brown, Yonghong Xie, Benedict T. Green, and Mark Lyte. 2003. "Catecholamines Modulate Escherichia Coli O157:H7 Adherence to Murine Cecal Mucosa." *Shock (Augusta, Ga.)*. doi: 10.1097/01.shk.0000073867.66587.e0.

Cogan, T. A., A. O. Thomas, L. E. N. Rees, A. H. Taylor, M. A. Jepson, P. H. Williams, J. Ketley, and T. J. Humphrey. 2007. "Norepinephrine Increases the Pathogenic Potential of Campylobacter Jejuni." *Gut*. doi: 10.1136/gut.2006.114926.

Cuskey, S. M., and R. H. Olsen. 1988. "Catabolism of Aromatic Biogenic Amines by Pseudomonas Aeruginosa PAO1 via Meta Cleavage of Homoprotocatechuic Acid."

Journal of Bacteriology. doi: 10.1128/jb.170.1.393-399.1988.

Cutler, Adele, and Leo Breiman. 1994. "Archetypal Analysis." *Technometrics*. doi: 10.1080/00401706.1994.10485840.

Edgar, Robert C. 2013. "UPARSE: Highly Accurate OTU Sequences from Microbial Amplicon Reads." *Nature Methods*. doi: 10.1038/nmeth.2604.

Eisenhofer, Graeme, Ånders Aneman, Peter Friberg, Douglas Hooper, Lars Fåndriks, Hans Lonroth, Béla Hunyady, and Eva Mezey. 1997. "Substantial Production of Dopamine in the Human Gastrointestinal Tract." *Journal of Clinical Endocrinology and Metabolism*. doi: 10.1210/jcem.82.11.4339.

Freestone, Primrose P. E., Richard D. Haigh, Peter H. Williams, and Mark Lyte. 1999. "Stimulation of Bacterial Growth by Heat-Stable, Norepinephrine-Induced Autoinducers." *FEMS Microbiology Letters*. doi: 10.1016/S0378-1097(99)00007-5.

Freestone, Primrose P. E., Sara M. Sandrini, Richard D. Haigh, and Mark Lyte. 2008. "Microbial Endocrinology: How Stress Influences Susceptibility to Infection." *Trends in Microbiology*.

Gao, Jinwei, Bingwen Xi, Kai Chen, Rui Song, Ting Qin, Jun Xie, and Liangkun Pan. 2019. "The Stress Hormone Norepinephrine Increases the Growth and Virulence of Aeromonas Hydrophila." *MicrobiologyOpen*. doi: 10.1002/mbo3.664.

Hintermayer, Sarah Beate, and Dirk Weuster-Botz. 2017. "Experimental Validation of in Silico Estimated Biomass Yields of Pseudomonas Putida KT2440." *Biotechnology Journal*. doi: 10.1002/biot.201600720.

Holmström, Kira M., and Toren Finkel. 2014. "Cellular Mechanisms and Physiological Consequences of Redox-Dependent Signalling." *Nature Reviews Molecular Cell Biology*.

Imlay, James A. 2013. "The Molecular Mechanisms and Physiological Consequences of Oxidative Stress: Lessons from a Model Bacterium." *Nature Reviews Microbiology*.

Kinney, Kevin S., Catherine E. Austin, Darla S. Morton, and Gerald Sonnenfeld. 2000. "Norepinephrine as a Growth Stimulating Factor in Bacteria - Mechanistic Studies." *Life Sciences*. doi: 10.1016/S0024-3205(00)00891-2.

Lewis, Nathan E., Kim K. Hixson, Tom M. Conrad, Joshua A. Lerman, Pep Charusanti, Ashoka D. Polpitiya, Joshua N. Adkins, Gunnar Schramm, Samuel O. Purvine, Daniel Lopez-Ferrer, Karl K. Weitz, Roland Eils, Rainer König, Richard D. Smith, and Bernhard Palsson. 2010. "Omic Data from Evolved E. Coli Are Consistent with Computed Optimal Growth from Genome-Scale Models." *Molecular Systems Biology*. doi: 10.1038/msb.2010.47.

Luengo, José M., and Elías R. Olivera. 2020. "Catabolism of Biogenic Amines in Pseudomonas Species." *Environmental Microbiology*.

Lyte, Mark. 2013. "Microbial Endocrinology in the Microbiome-Gut-Brain Axis: How Bacterial Production and Utilization of Neurochemicals Influence Behavior." *PLoS Pathogens*. doi: 10.1371/journal.ppat.1003726.

Lyte, Mark, Cory D. Frank, and Ben T. Green. 1996. "Production of an Autoinducer of Growth by Norepinephrine Cultured Escherichia Coli O157:H7." *FEMS Microbiology Letters*. doi: 10.1016/0378-1097(96)00135-8.

Maggiorani, Damien, Nicola Manzella, Dale E. Edmondson, Andrea Mattevi, Angelo Parini, Claudia Binda, and Jeanne Mialet-Perez. 2017. "Monoamine Oxidases, Oxidative Stress, and Altered Mitochondrial Dynamics in Cardiac Ageing." *Oxidative Medicine and Cellular Longevity*.

McDonald, Daniel, Morgan N. Price, Julia Goodrich, Eric P. Nawrocki, Todd Z. Desantis, Alexander Probst, Gary L. Andersen, Rob Knight, and Philip Hugenholtz. 2012. "An Improved Greengenes Taxonomy with Explicit Ranks for Ecological and Evolutionary Analyses of Bacteria and Archaea." *ISME Journal*. doi: 10.1038/ismej.2011.139.

Metsalu, Tauno, and Jaak Vilo. 2015. "ClustVis: A Web Tool for Visualizing Clustering of Multivariate Data Using Principal Component Analysis and Heatmap." *Nucleic Acids Research*. doi: 10.1093/nar/gkv468.

Nagpal, Sunil, Mohammed Monzoorul Haque, Rashmi Singh, and Sharmila S. Mande. 2019. "IVikodak-A Platform and Standard Workflow for Inferring, Analyzing, Comparing, and Visualizing the Functional Potential of Microbial Communities." *Frontiers in Microbiology*. doi: 10.3389/fmicb.2018.03336.

Nakano, M., A. Takahashi, Y. Sakai, M. Kawano, N. Harada, K. Mawatari, and Y. Nakaya. 2007. "Catecholamine-Induced Stimulation of Growth in Vibrio Species." *Letters in Applied Microbiology*. doi: 10.1111/j.1472-765X.2007.02136.x.

Neri, Margherita, Daniela Cerretani, Anna Ida Fiaschi, Pasini Franco Laghi, Pietro Enea Lazzerini, Angela Bruna Maffione, Lucia Micheli, Giancarlo Bruni, Cristina Nencini, O. Giorgi, Stefano D'Errico, Carmela Fiore, Cristoforo Pomara, Irene Riezzo, Emanuela Turillazzi, and Vittorio Fineschi. 2007. "Correlation between Cardiac Oxidative Stress and Myocardial Pathology Due to Acute and Chronic Norepinephrine Administration in Rats." *Journal of Cellular and Molecular Medicine*. doi: 10.1111/j.1582-4934.2007.00009.x.

Nogales, Juan, Joshua Mueller, Steinn Gudmundsson, Francisco J. Canalejo, Estrella Duque, Jonathan Monk, Adam M. Feist, Juan Luis Ramos, Wei Niu, and Bernhard O. Palsson. 2020. "High-Quality Genome-Scale Metabolic Modelling of Pseudomonas Putida Highlights Its Broad Metabolic Capabilities." *Environmental Microbiology*. doi: 10.1111/1462-2920.14843.

Quast, Christian, Elmar Pruesse, Pelin Yilmaz, Jan Gerken, Timmy Schweer, Pablo Yarza, Jörg Peplies, and Frank Oliver Glöckner. 2013. "The SILVA Ribosomal RNA Gene Database Project: Improved Data Processing and Web-Based Tools." *Nucleic Acids Research*. doi: 10.1093/nar/gks1219.

Saller, S., J. Merz-Lange, S. Raffael, S. Hecht, R. Pavlik, C. Thaler, D. Berg, U. Berg, L. Kunz, and Arthur Mayerhofer. 2012. "Norepinephrine, Active Norepinephrine Transporter, and Norepinephrine- Metabolism Are Involved in the Generation of Reactive Oxygen Species in Human Ovarian Granulosa Cells." *Endocrinology*. doi: 10.1210/en.2011-1769.

Sandrini, Sara, Fayez Alghofaili, Primrose Freestone, and Hasan Yesilkaya. 2014. "Host Stress Hormone Norepinephrine Stimulates Pneumococcal Growth, Biofilm Formation and Virulence Gene Expression." *BMC Microbiology*. doi: 10.1186/1471-2180-14-180.

Sarkodie, Emmanuel Konadu, Shuxin Zhou, Sarah Ama Baidoo, and Weihua Chu. 2019. "Influences of Stress Hormones on Microbial Infections." *Microbial Pathogenesis*.

Siddiqui, Aarif, and Paolo Ceppi. 2020. "A Non-Proliferative Role of Pyrimidine Metabolism

in Cancer." *Molecular Metabolism*.

Sies, Helmut. 2017. "Hydrogen Peroxide as a Central Redox Signaling Molecule in Physiological Oxidative Stress: Oxidative Eustress." *Redox Biology*.

Sies, Helmut, and Dean P. Jones. 2020. "Reactive Oxygen Species (ROS) as Pleiotropic Physiological Signalling Agents." *Nature Reviews Molecular Cell Biology*.

Thannickal, Victor J., and Barry L. Fanburg. 2000. "Reactive Oxygen Species in Cell Signaling." *American Journal of Physiology - Lung Cellular and Molecular Physiology*.

Truccollo, Brendha, Paul Whyte, and Declan J. Bolton. 2020. "An Investigation of the Effect of Catecholamines and Glucocorticoids on the Growth and Pathogenicity of Campylobacter Jejuni." *Pathogens*. doi: 10.3390/pathogens9070555.

Wang, Qiong, George M. Garrity, James M. Tiedje, and James R. Cole. 2007. "Naïve Bayesian Classifier for Rapid Assignment of RRNA Sequences into the New Bacterial Taxonomy." *Applied and Environmental Microbiology*. doi: 10.1128/AEM.00062-07.

Xu, Fuzhou, Cun Wu, Fangfang Guo, Guolin Cui, Ximin Zeng, Bing Yang, and Jun Lin. 2015. "Transcriptomic Analysis of Campylobacter Jejuni NCTC 11168 in Response to Epinephrine and Norepinephrine." *Frontiers in Microbiology*. doi: 10.3389/fmicb.2015.00452.

Yang, Laurence, Nathan Mih, Amitesh Anand, Joon Ho Park, Justin Tan, James T. Yurkovich, Jonathan M. Monk, Colton J. Lloyd, Troy E. Sandberg, Sang Woo Seo, Donghyuk Kim, Anand V. Sastry, Patrick Phaneuf, Ye Gao, Jared T. Broddrick, Ke Chen, David Heckmann, Richard Szubin, Ying Hefner, Adam M. Feist, and Bernhard O. Palsson. 2019. "Cellular Responses to Reactive Oxygen Species Are Predicted from Molecular Mechanisms." *Proceedings of the National Academy of Sciences of the United States of America*. doi: 10.1073/pnas.1905039116.

Zhou, Mian, H. Hank Simms, and Ping Wang. 2004. "Increased Gut-Derived Norepinephrine Release in Sepsis: Up-Regulation of Intestinal Tyrosine Hydroxylase." *Biochimica et Biophysica Acta - Molecular Basis of Disease*. doi: 10.1016/j.bbadis.2004.03.008.